Synthesis, characterization and use of benzothioxanthene imide based dimers

José María Andrés Castán,[a]† Clément Dalinot,[a]† Sergey Dayneko,[b] Laura Abad Galan,[c] Pablo Simón Marqués,[a] Olivier Alévêque,[a] Magali Allain,[a] Olivier Maury,[c] Ludovic Favereau,[d] Philippe Blanchard,[a] Gregory Welch, *[b] and Clément Cabanetos*[a]

[a] CNRS UMR 6200, MOLTECH-Anjou, University of Angers, 2 Bd Lavoisier, 49045 Angers, France.

[b] Department of Chemistry, University of Calgary, 2500 University Drive N.W., Calgary, Alberta T2N 1N4, Canada.

[c] Univ Lyon, ENS de Lyon, CNRS UMR 5182, Université Claude Bernard Lyon 1, F-69342 Lyon, France.
Univ Rennes, CNRS, ISCR – UMR 6226, ScanMAT – UMS 2001, F-35000 Rennes, France.

† both authors equally contributed to this work

Table of contents

General information

All reagents and chemicals from commercial sources were used without further purification. Solvents were dried and purified using standard techniques. Flash chromatography was performed with analytical-grade solvents using Aldrich silica gel (technical grade, pore size 60 Å, 230-400 mesh particle size). Flexible plates ALUGRAM® Xtra SIL G UV254 from MACHEREY-NAGEL were used for TLC. Compounds were detected by UV irradiation (Bioblock Scientific). NMR spectra were recorded with a Bruker AVANCE III 300 (^{1}H, 300 MHz and ^{13}C, 75MHz) or a Bruker AVANCE DRX500 (^{1}H, 500 MHz; ^{13}C, 125 MHz). Chemical shifts are given in ppm relative to TMS and coupling constants J in Hz. Matrix Assisted Laser Desorption/Ionization was performed on MALDI-TOF MS BIFLEX III Bruker Daltonics spectrometer using DCTB+ as matrix. High resolution mass spectrometry (HRMS) was performed with a JEOL JMS-700 B/E. Cyclic voltammetry was performed using a Biologic SP-150 potentiostat with positive feedback compensation in 0.10 M Bu_4NPF_6/CH_2Cl_2 (HPLC grade). Experiments were carried out in a one-compartment cell equipped with a platinum working electrode (2 mm of diameter) and a platinum wire counter electrode. A silver wire immersed in 0.10 M Bu_4NPF_6/CH_2Cl_2 was used as pseudo-reference electrode and checked against the ferrocene/ferrocenium couple (Fc/Fc^+) before and after each experiment. The potentials were then expressed vs Fc/Fc^+.

Synthetic procedures

BTXI-Br and **BTXI-SO_2-Br** were synthesized according to our previously described procedures.[1]

5-isobutyl-2-(pentan-3-yl)-1*H*-thioxantheno[2,1,9-*def*]isoquinoline-1,3(2*H*)-dione (BTXI-Alk)

Dry toluene (5 mL) was added to a mixture of $PdCl_2$(dppf) (16 mg, 22 µmol), isobutylboronic acid (90 mg, 0.88 mmol), **BTXI-Br** (200 mg, 0.44 mmol), and K_2CO_3 (183 mg, 1.3 mmol) and the resulting mixture was heated under reflux for 16 h. After removing the solvent under vacuum, the residue was dissolved in CH_2Cl_2 and this organic phase was washed with brine and dried over $MgSO_4$ prior to removing the solvent under vacuum. The crude was purified by flash column chromatography (eluent: toluene) to afford **BTXI-Alk** as an orange solid (140 mg, 74%).

^{1}H NMR (300 MHz, $CDCl_3$): δ (ppm) 8.57 (d, J = 8.1 Hz, 1H), 8.33 (s, 1H), 8.26 – 8.18 (m, 2H), 7.47 – 7.35 (m, 3H), 5.14 – 4.98 (m, 1H), 2.74 (d, J = 7.2 Hz, 2H), 2.36 – 2.12 (m, 3H), 1.99 – 1.81 (m, 2H), 1.05 (d, J = 6.6 Hz, 6H), 0.90 (t, J = 7.5 Hz, 6H). ^{13}C NMR (75 MHz, $CDCl_3$): δ (ppm) 137.9, 136.4, 132.7, 131.9, 129.8, 129.3, 128.1, 127.7, 126.9, 126.2, 126.1, 119.5, 57.4, 43.3, 27.3, 25.1, 22.9, 11.5. HRMS (EI): *m/z* calcd for $C_{27}H_{27}NO_2S$: 429.1757, found 429.1752.

11-bromo-5-isobutyl-2-(pentan-3-yl)-1*H*-thioxantheno[2,1,9-*def*]isoquinoline-1,3(2*H*)-dione (Br-BTXI)

To a solution of **BTXI-Alk** (1.0 g, 2.3 mmol) in $CHCl_3$ (50 mL) was added dropwise bromine (300 µL, 5.8 mmol). The reaction mixture was refluxed for 16 h before being quenched with a saturated aqueous solution of $Na_2S_2O_3$. Then, the organic phase was washed with water and brine. After drying it over $MgSO_4$, the solution was concentrated under reduced pressure and the crude was purified by column chromatography on silica gel (eluent: toluene). Yield: orange solid (860 mg, 73%).

^{1}H NMR (300 MHz, $CDCl_3$): δ (ppm) 8.80 (s, 1H), 8.66 – 8.60 (m, 1H), 8.31 (s, 1H), 7.58 – 7.52 (m, 1H), 7.46 – 7.34 (m, 2H), 5.09 – 4.95 (m, 1H), 2.82 (d, J = 7.3 Hz, 2H), 2.33 – 2.10 (m, 3H), 1.98 – 1.82 (m, 2H), 1.02 (d, J = 6.6 Hz, 6H), 0.89 (t, J = 7.5 Hz, 6H). ^{13}C NMR (75 MHz, $CDCl_3$) δ 136.9, 136.7, 134.6, 133.4, 131.1, 130.5, 129.9, 128.9, 127.1, 126.4, 117.3, 57.7, 43.9, 28.1, 25.1, 22.8, 11.5. HRMS (EI): *m/z* calcd for $C_{27}H_{26}BrNO_2S$: 507.0862, found 507.0859.

General procedure for the copper-catalyzed Ullmann reactions

A mixture of the respective brominated BTXI (300 mg, 1 eq) and copper powder (10 eq) in dry DMSO (10 mL) was stirred under argon at the indicated temperature for the appropriate period of time. After that, the mixture was filtered on a silica plug and the mixture was extracted with ethyl acetate. The organic layer was washed with brine and water, dried over $MgSO_4$ and then the solvent was removed under reduced pressure.

2,2'-di(pentan-3-yl)-1*H*,1'*H*-[5,5'-bithioxantheno[2,1,9-*def*]isoquinoline]-1,1',3,3'(2*H*,2'*H*)-tetraone (D1)

Following the general procedure over **BTXI-Br** at 100 °C for 16 h, **D1** was obtained as an orange powder after purification via column chromatography on silica gel (eluent: CH_2Cl_2). (40% yield).

^{1}H NMR (500 MHz, $CDCl_3$): δ (ppm) 8.72 (d, *J* = 8.3 Hz, 2H), 8.40 (s, 2H), 8.34 (d, *J* = 8.3 Hz, 2H), 8.28 (dd, *J* = 8.5, 1.2 Hz, 2H), 7.41 (ddd, *J* = 8.5, 7.1, 1.4 Hz, 2H), 7.33 (ddd, *J* = 8.2, 7.1, 1.2 Hz, 2H), 7.21 (dd, *J* = 8.2, 1.4 Hz, 2H), 5.13 – 5.03 (m, 2H), 2.34 – 2.20 (m, 4H), 2.00 – 1.88 (m, 4H), 0.94 (t, *J* = 7.4 Hz, 12H). ^{13}C NMR (125 MHz, $CDCl_3$): δ (ppm) 140.4, 137.0, 133.1, 131.9, 130.6, 130.0, 129.5, 128.0, 127.9, 127.0, 126.6, 126.2, 119.9, 57.7, 25.1, 11.6. HRMS (FAB): *m/z* calcd for $C_{46}H_{36}N_2O_4S_2$: 744.2111, found 744.2104. Monocrystals were obtained by slow evaporation of chloroform.

2,2'-di(pentan-3-yl)-1*H*,1'*H*-[5,5'-bithioxantheno[2,1,9-*def*]isoquinoline]-1,1',3,3'(2*H*,2'*H*)-tetraone 6,6,6',6'-tetraoxide (D2)

Following the general procedure over **BTXI-SO_2-Br** at 150 °C for 6 h, **D2** was obtained as a yellow powder after purification via recycling HPLC and precipitation from $CHCl_3$/pentane. (72% yield).

^{1}H NMR (500 MHz, $CDCl_3$): δ (ppm) 8.86 – 8.81 (m, 4H), 8.70 (d, *J* = 8.1 Hz, 2H), 8.28 (dd, *J* = 8.4, 1.0 Hz, 2H), 8.01 (dd, *J* = 8.0, 1.4 Hz, 2H), 7.77 (ddd, *J* = 8.4, 7.3, 1.4 Hz, 2H), 7.60 (ddd, *J* = 8.0, 7.3, 1.0 Hz, 2H), 5.07 – 4.99 (m, 2H), 2.29 – 2.16 (m, 4H), 1.99 – 1.88 (m, 4H), 0.94 (t, *J* = 7.5 Hz, 12H). ^{13}C NMR (125 MHz, $CDCl_3$): δ (ppm) 136.5, 136.5, 135.6, 134.1, 133.7, 132.4, 131.2, 131.0, 130.7, 128.9, 126.5, 126.1, 124.8, 124.3, 58.4, 25.1, 11.6. HRMS (FAB): *m/z* calcd for $C_{46}H_{36}N_2O_8S_2$: 808.1908, found 808.1913. Monocrystals were obtained by slow evaporation of chloroform.

5,5'-diisobutyl-2,2'-di(pentan-3-yl)-1*H*,1'*H*-[11,11'-bithioxantheno[2,1,9-*def*]isoquinoline]-1,1',3,3'(2*H*,2'*H*)-tetraone (D3)

Following the general procedure over **Br-BTXI** at 200 °C for 16 h, **D3** was obtained as an orange powder after purification via column chromatography on silica gel (eluent: CH_2Cl_2). (45% yield).

^{1}H NMR (300 MHz, $CDCl_3$): δ (ppm) 8.60 (s, 2H), 8.35 (s, 2H), 7.42 – 7.33 (m, 4H), 7.19 (ddd, *J* = 7.9, 7.6, 1.0 Hz, 2H), 6.71 (ddd, *J* = 7.8, 7.6, 1.2 Hz, 2H), 5.07 – 4.94 (m, 2H), 2.83 (d, *J* = 7.2 Hz, 4H), 2.30 – 2.12 (m, 6H), 1.99 – 1.80 (m, 4H), 1.10 – 0.99 (m, 12H), 0.89 (t, *J* = 7.4 Hz, 12H). ^{13}C NMR (75 MHz, $CDCl_3$): δ (ppm) 137.6, 137.6, 135.4, 133.9, 133.3, 131.2, 129.8, 129.3, 128.6, 127.8, 127.1, 126.2, 57.6, 43.7, 28.0, 25.2, 22.9, 22.8, 11.5. HRMS (FAB): *m/z* calcd for $C_{54}H_{52}N_2O_4S_2$: 856.3363, found 856.3360. Monocrystals were obtained by slow evaporation of toluene.

Scheme S1. Pallado-catalyzed conditions for the synthesis of **D1**.

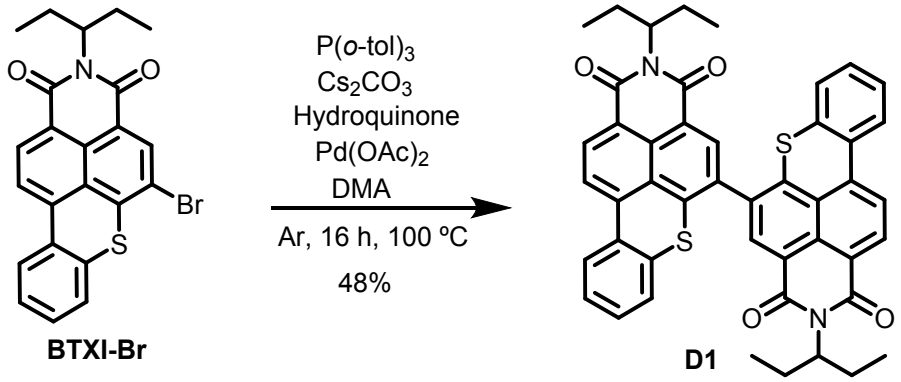

DMA (0.5 mL) was added to a mixture of BTXI-Br (100.0 mg, 0.22 mmol), hydroquinone (12.2 mg, 0.11 mmol), Cs_2CO_3 (79.2 mg, 0.24 mmol), P(*o*-tol)$_3$ (2.7 mg, 8.8 µmol) and $Pd(OAc)_2$ (2.0 mg, 8.8 µmol) under argon. After degassing during 20 minutes, the mixture was left to react at 100 °C during 16 h. Then, the reaction was quenched with water and the organic phase was extracted with CH_2Cl_2, dried with $MgSO_4$ and concentrated under reduced pressure. The product was purified by column chromatography on silica gel (eluent: CH_2Cl_2) yielding **D1** (40.1 mg, 49%) as an orange powder.

NMR and HRMS Spectra

Figure S1. ^{1}H NMR ($CDCl_3$, 300 MHz) spectrum of **BTXI-Alk**.

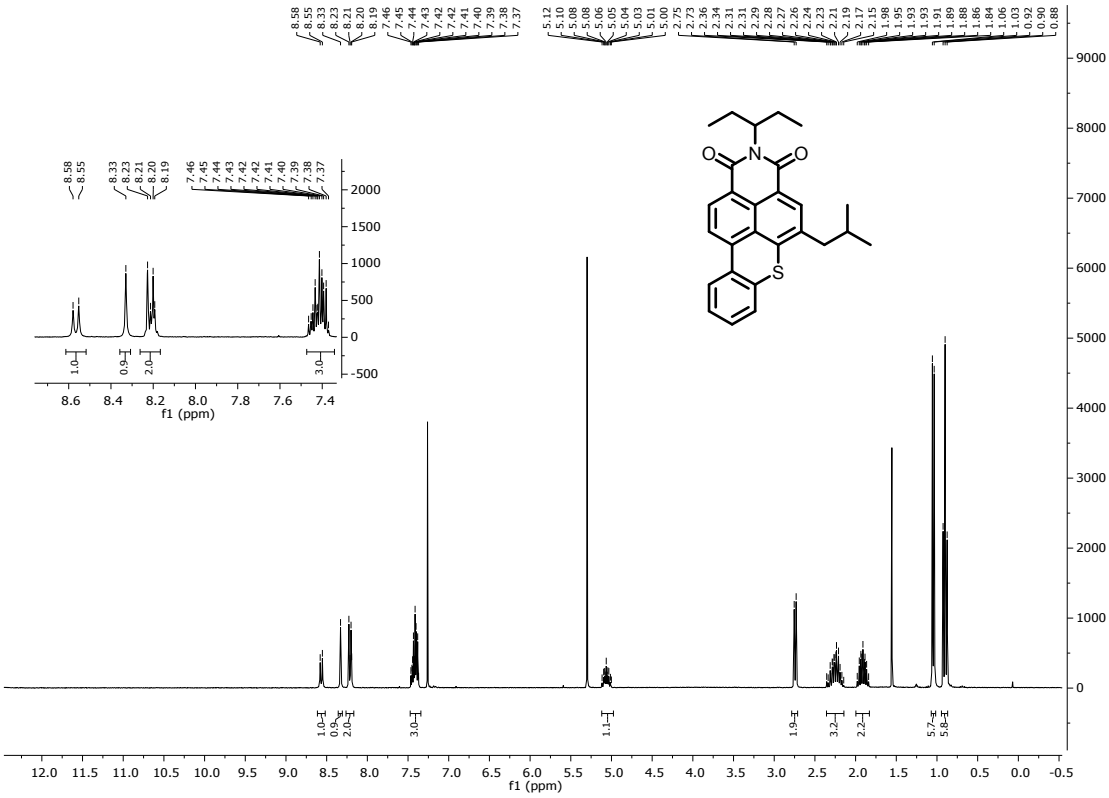

Figure S2. ^{13}C NMR ($CDCl_3$, 75 MHz) spectrum of **BTXI-Alk**.

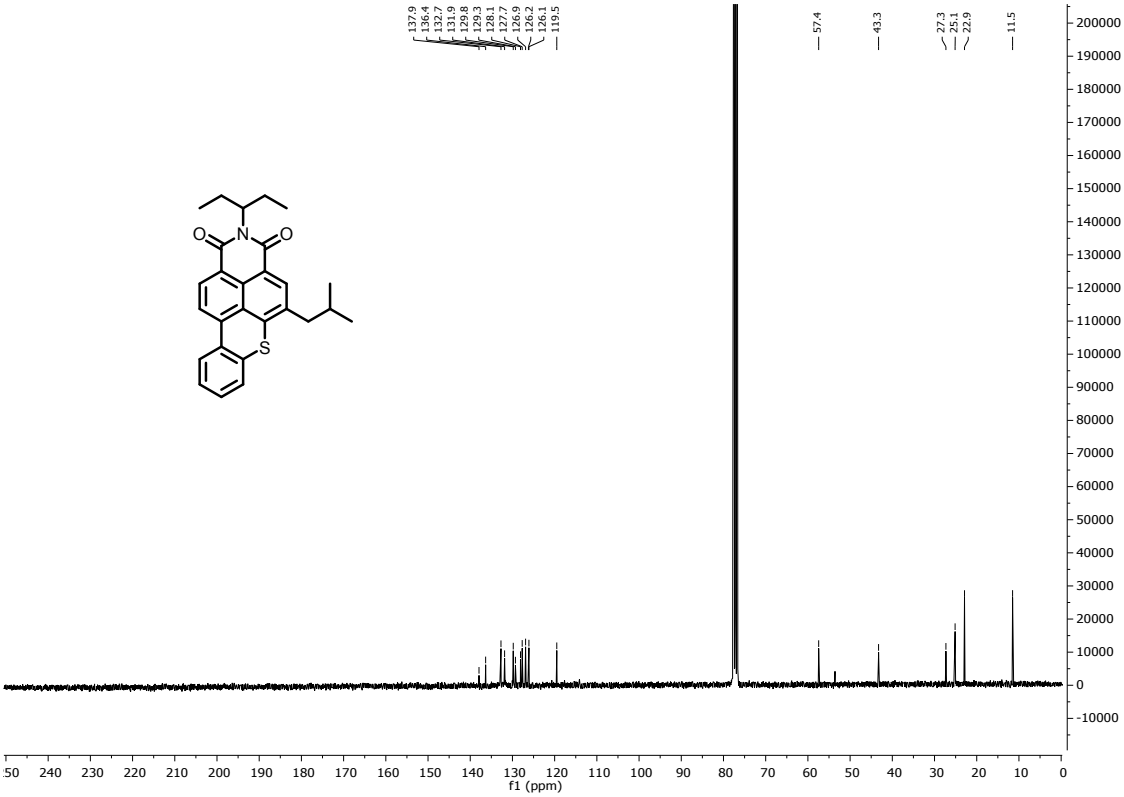

Figure S3. ^{1}H NMR ($CDCl_3$, 300 MHz) spectrum of **Br-BTXI**.

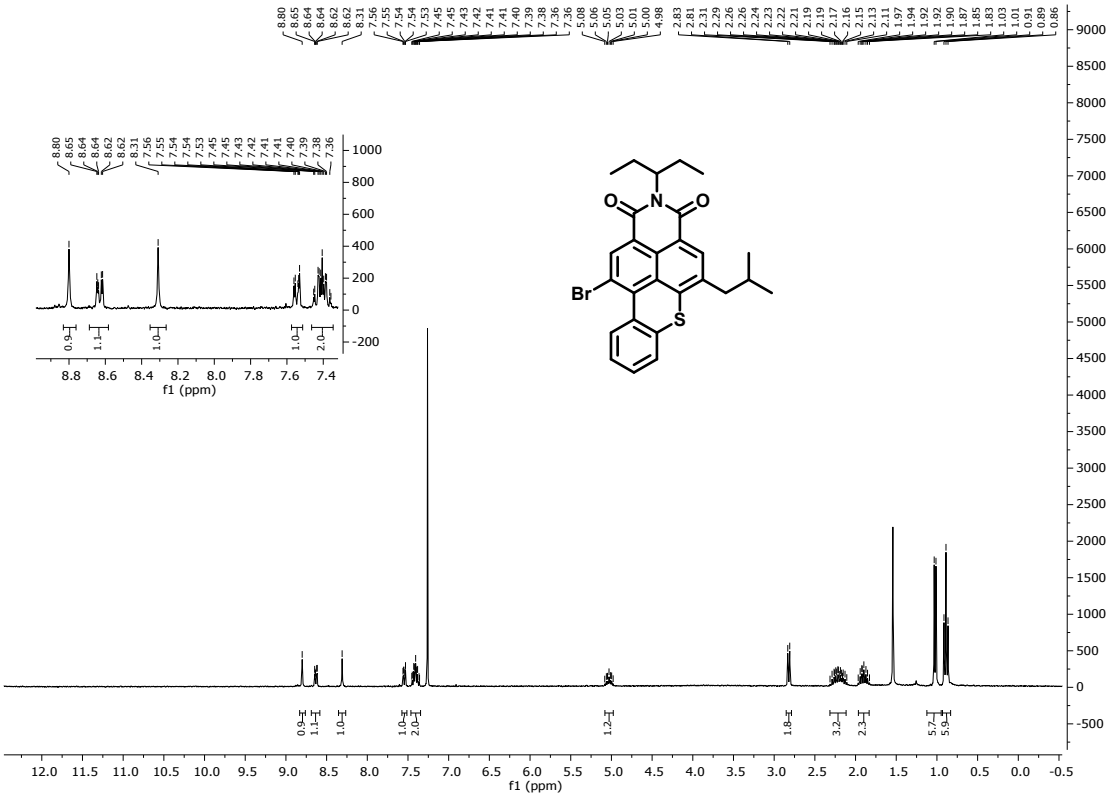

Figure S4. ^{13}C NMR ($CDCl_3$, 75 MHz) spectrum of **Br-BTXI**.

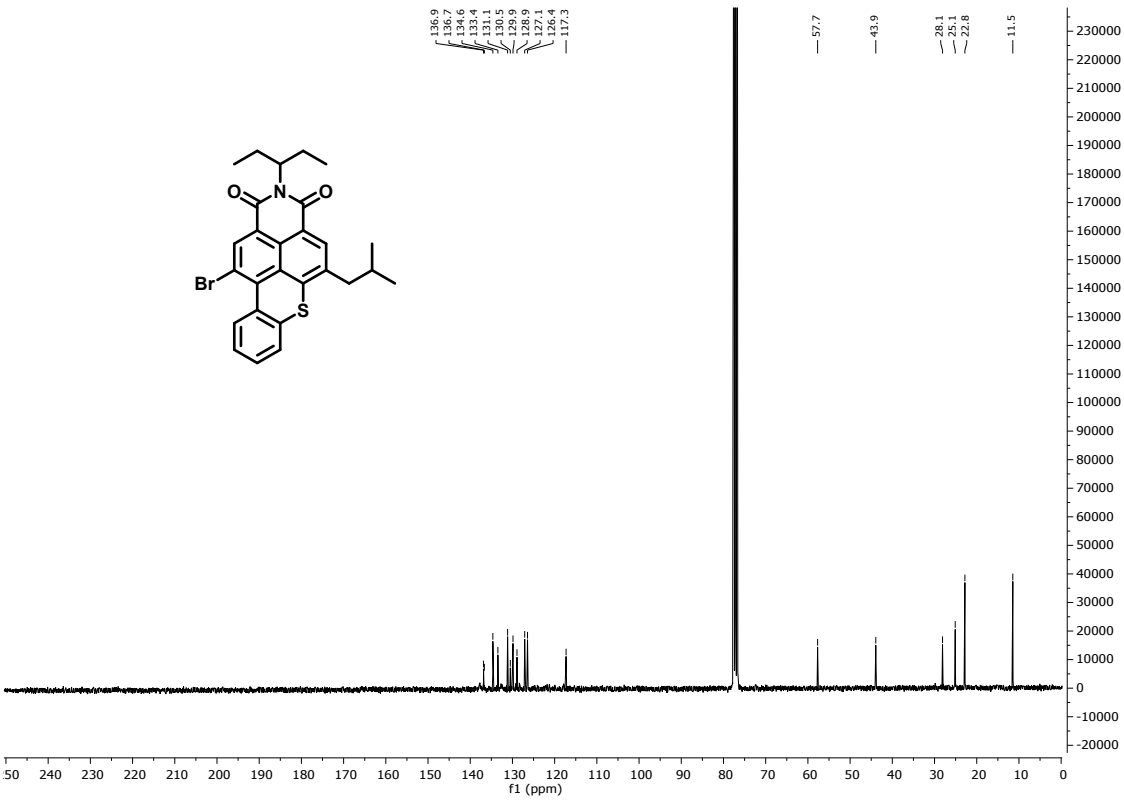

Figure S5. ^{1}H NMR ($CDCl_3$, 500 MHz) spectrum of **D1**.

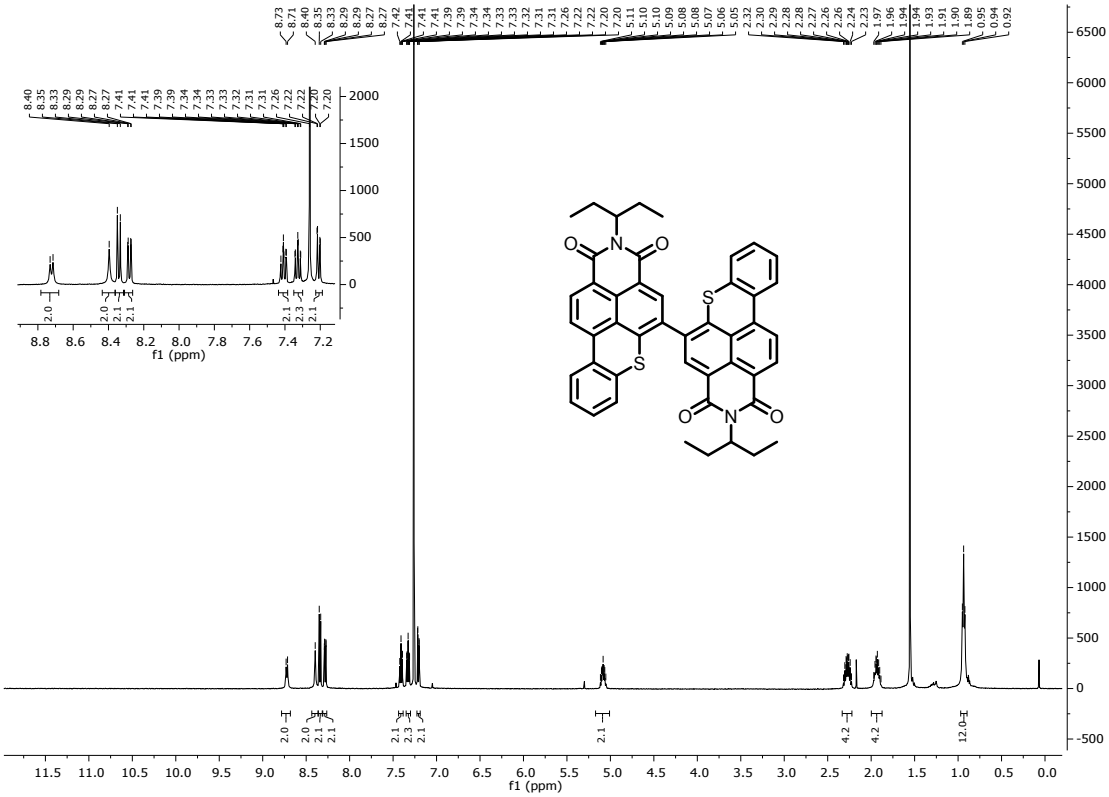

Figure S6. ^{13}C NMR ($CDCl_3$, 125 MHz) spectrum of **D1**.

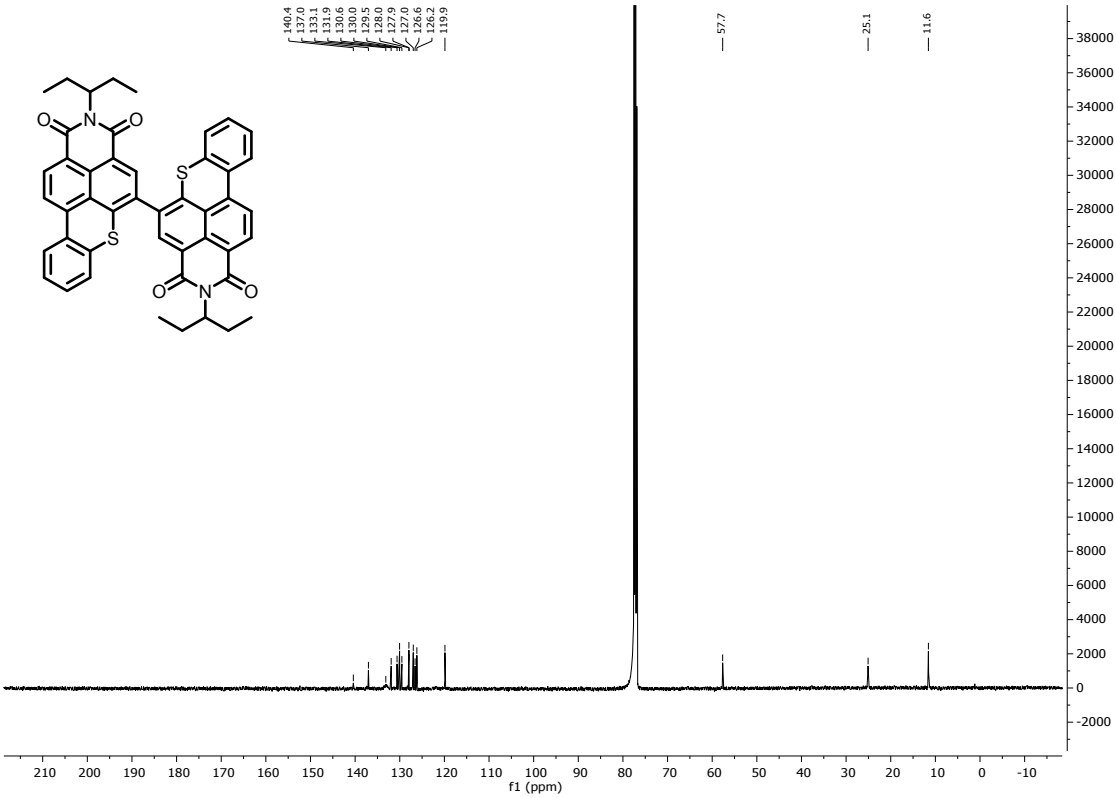

Figure S7. ^{1}H NMR ($CDCl_3$, 500 MHz) spectrum of **D2**.

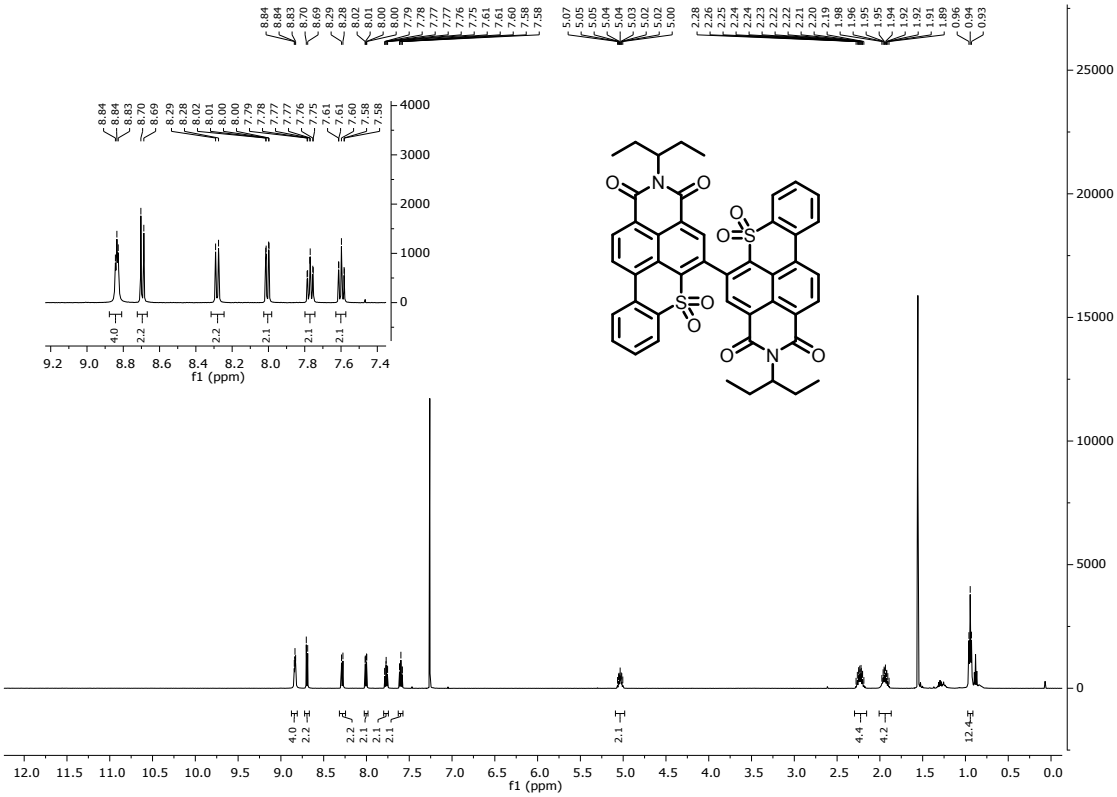

Figure S8. ^{13}C NMR ($CDCl_3$, 125 MHz) spectrum of **D2**.

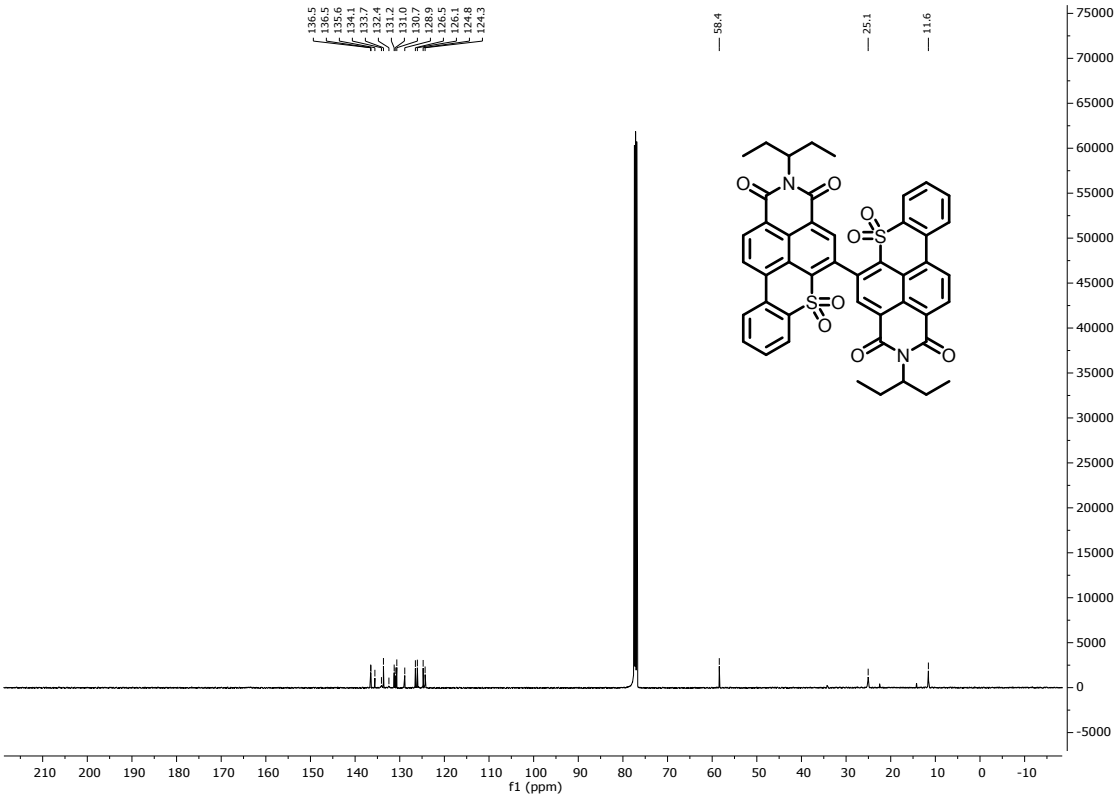

Figure S9. ^{1}H NMR ($CDCl_3$, 300 MHz) spectrum of **D3**.

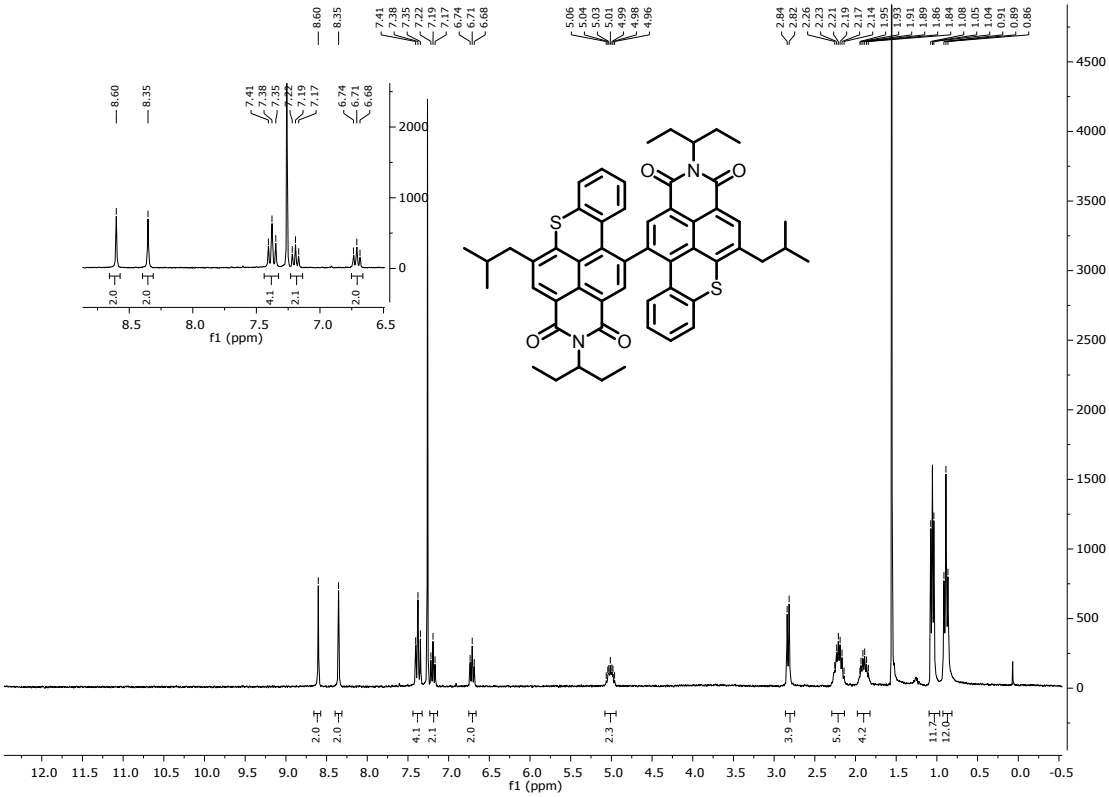

Figure S10. ^{13}C NMR ($CDCl_3$, 75 MHz) spectrum of **D3**.

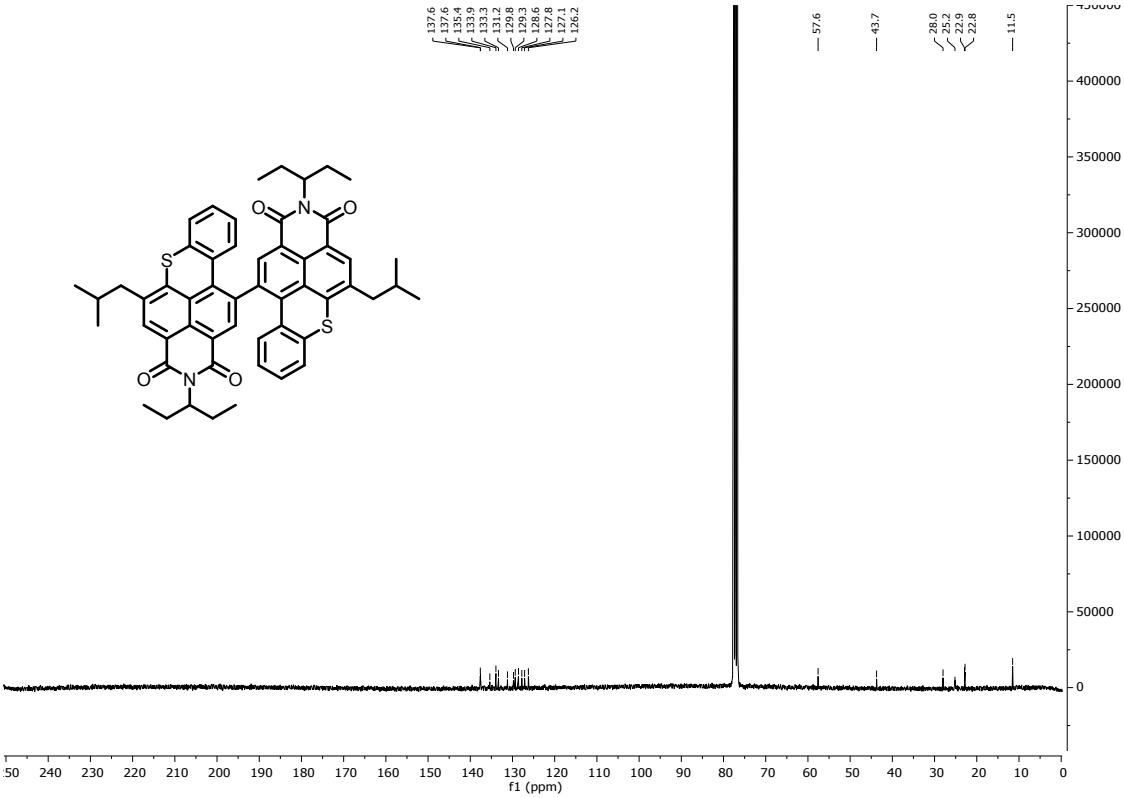

Figure S11. HRMS (EI) spectrum of **BTXI-Alk**: *m/z* calcd for $C_{27}H_{27}NO_2S$: 429.1757, found 429.1752.

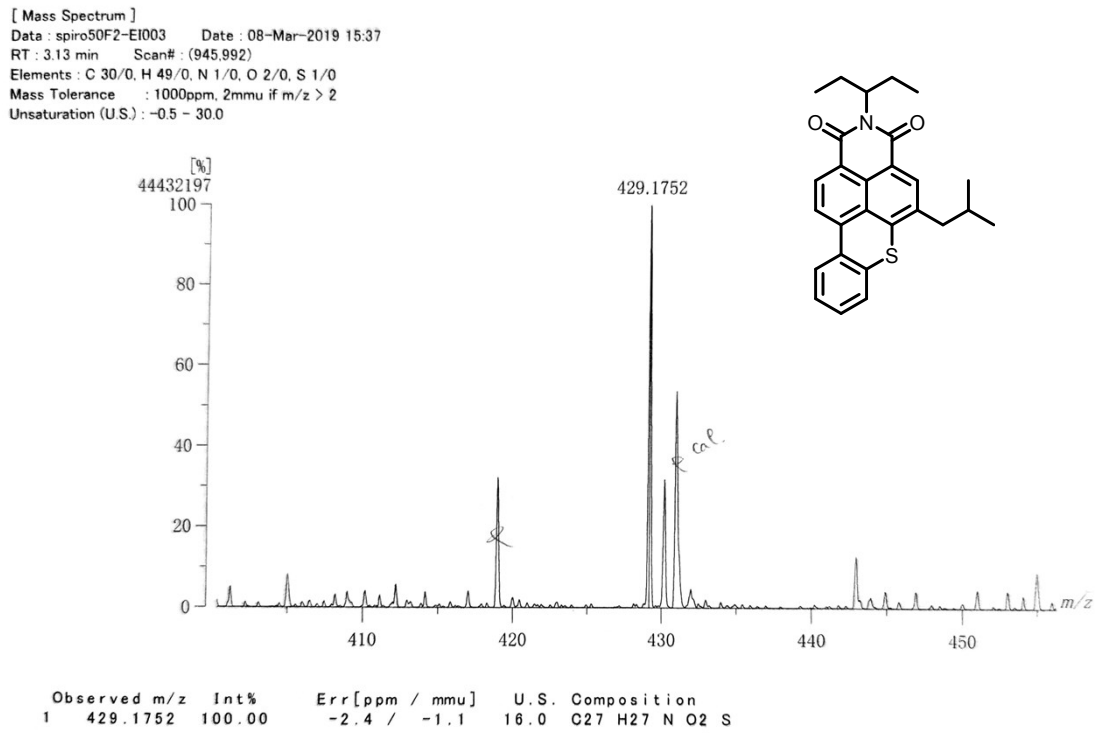

Figure S12. HRMS (EI) spectrum of **Br-BTXI**: *m/z* calcd for $C_{27}H_{26}BrNO_2S$: 507.0862, found 507.0859.

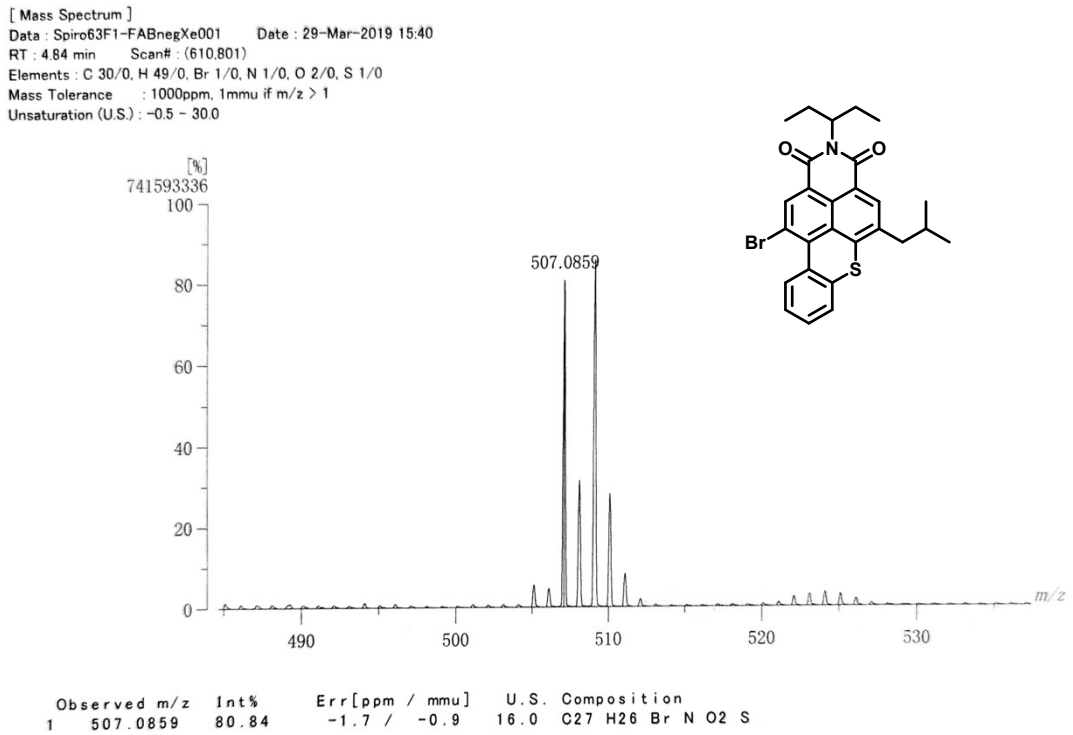

Figure S13. HRMS (FAB) spectrum of **D1**: *m/z* calcd for $C_{46}H_{36}N_2O_4S_2$: 744.2111, found 744.2104.

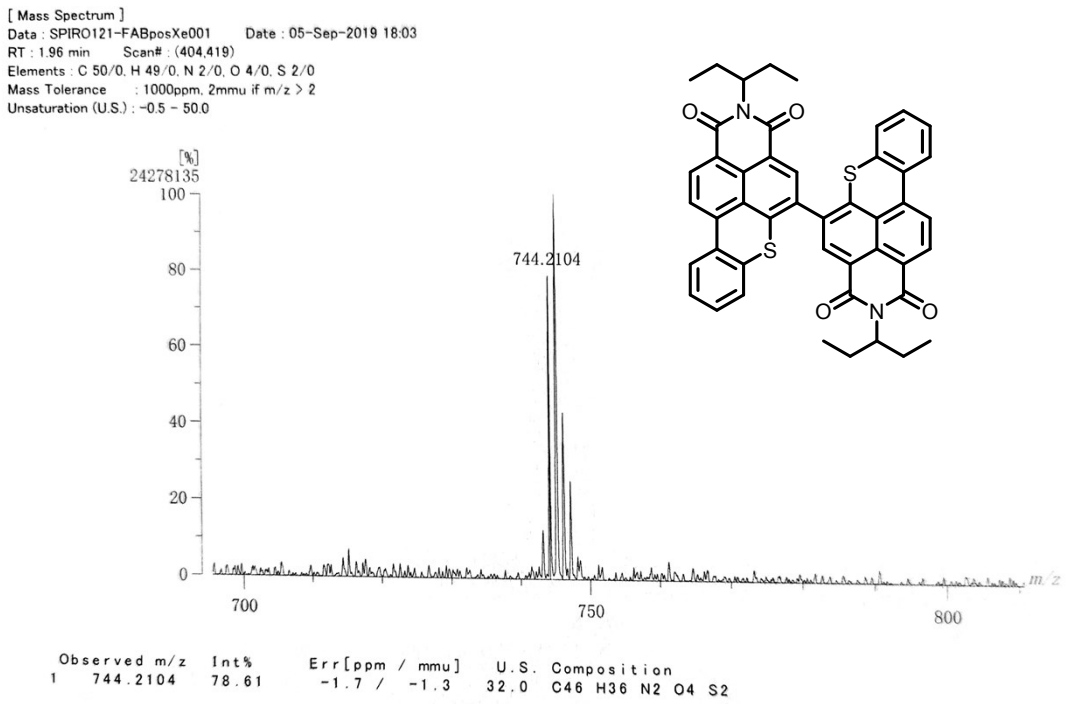

Figure S14. HRMS (FAB) spectrum of **D2**: *m/z* calcd for $C_{46}H_{36}N_2O_8S_2$: 808.1908, found 808.1913.

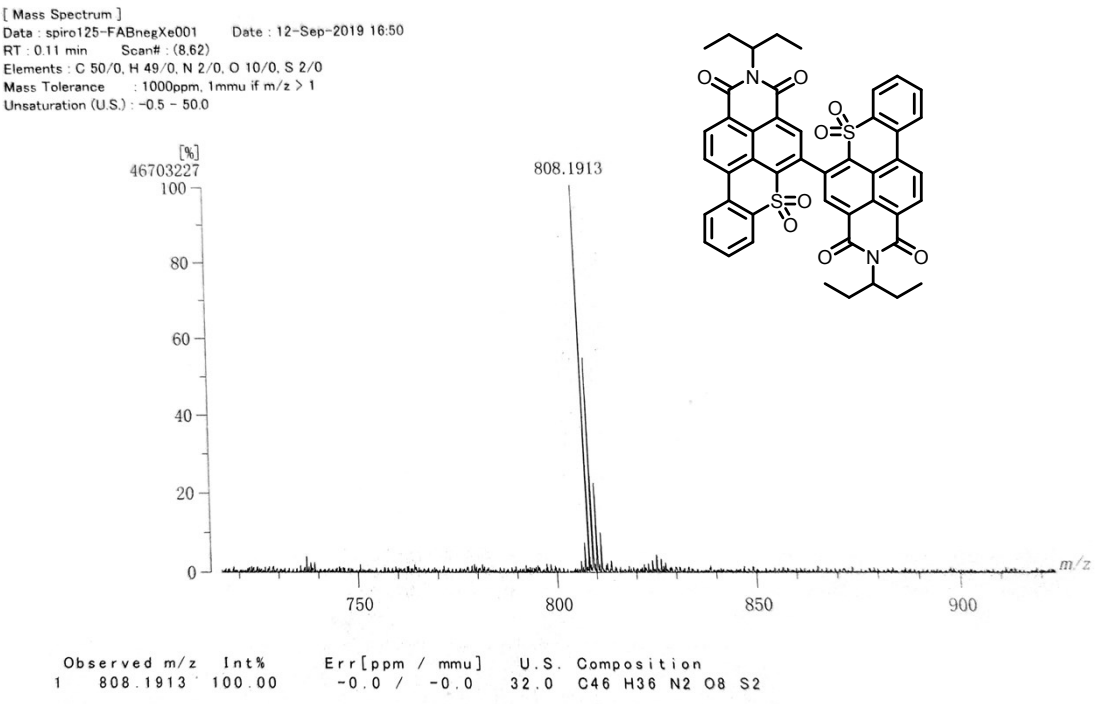

Figure S15. HRMS (FAB) spectrum of **D3**: *m/z* calcd for $C_{54}H_{52}N_2O_4S_2$: 856.3363, found 856.3360.

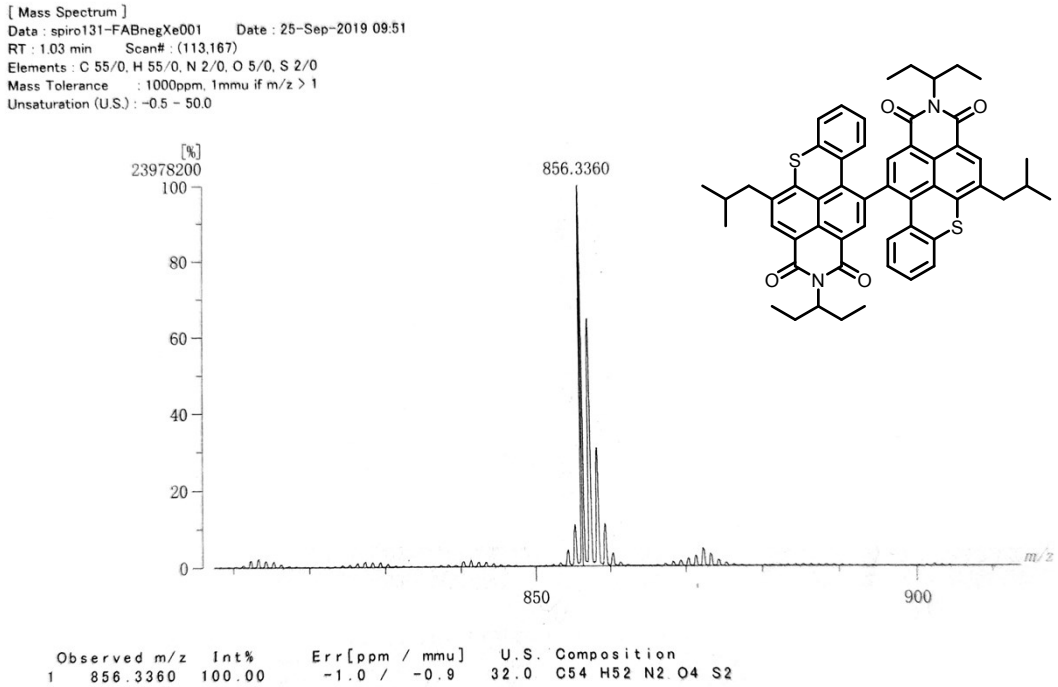

	Observed m/z	Int%	Err[ppm / mmu]	U.S.	Composition
1	856.3360	100.00	-1.0 / -0.9	32.0	C54 H52 N2 O4 S2

Optical characterization

Figure S16. Absorption spectra of dimers **D1**, **D2** and **D3** in dichloromethane.

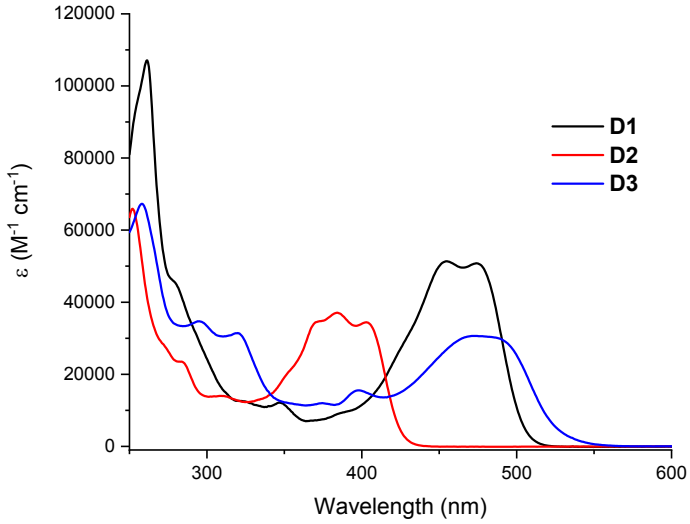

Figure S17. Emission spectra of dimers **D1**, **D2** and **D3** in dichloromethane.

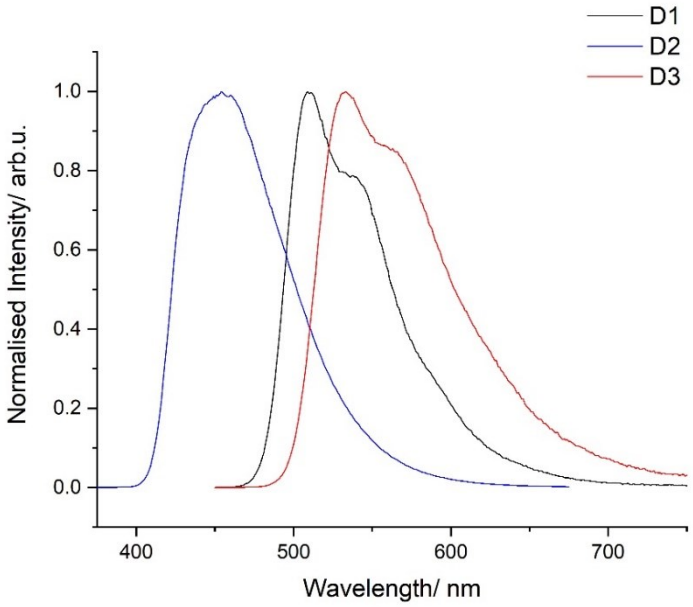

X-ray crystallography

Figure S.18. X-ray structures of **BTXI-Alk.**

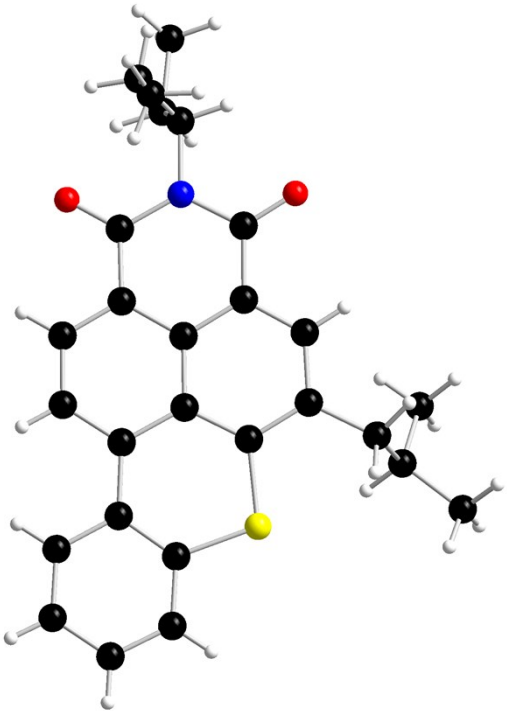

Figure S19. X-ray structures of **D1**, **D2** and **D3**, θ = dihedral angle of the bay area.

D1

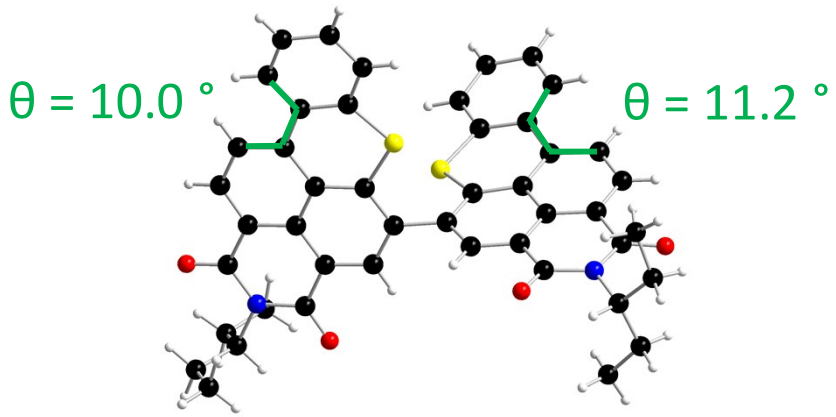

D2

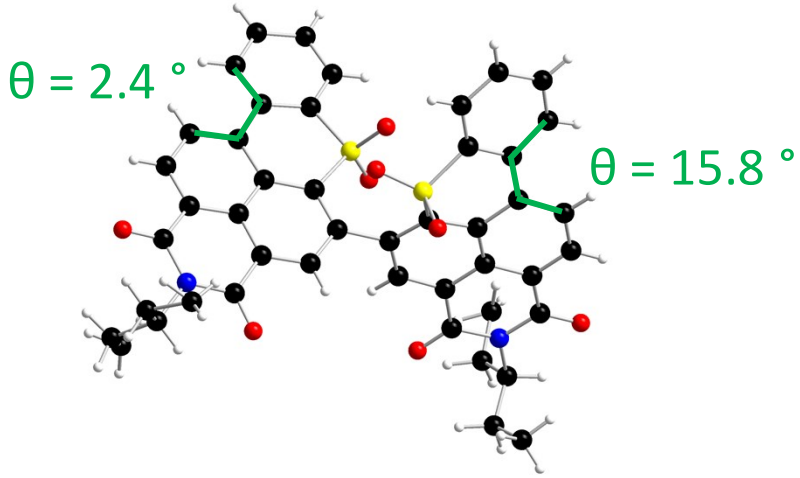

D3

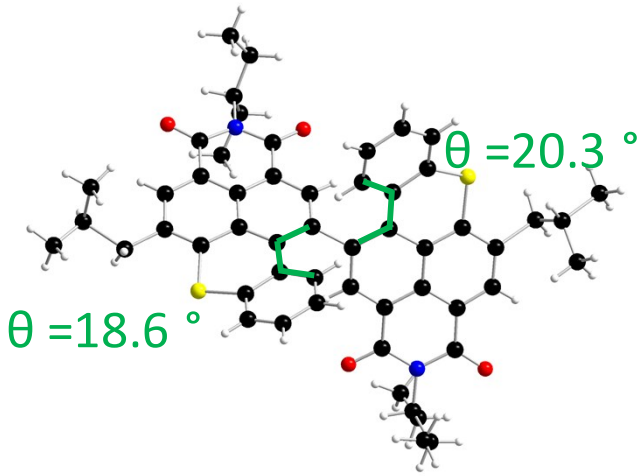

Figure S20. X-Ray structure of **BTXI** highlighting the head-to-tail packing and its π-π interaction distances in Å.

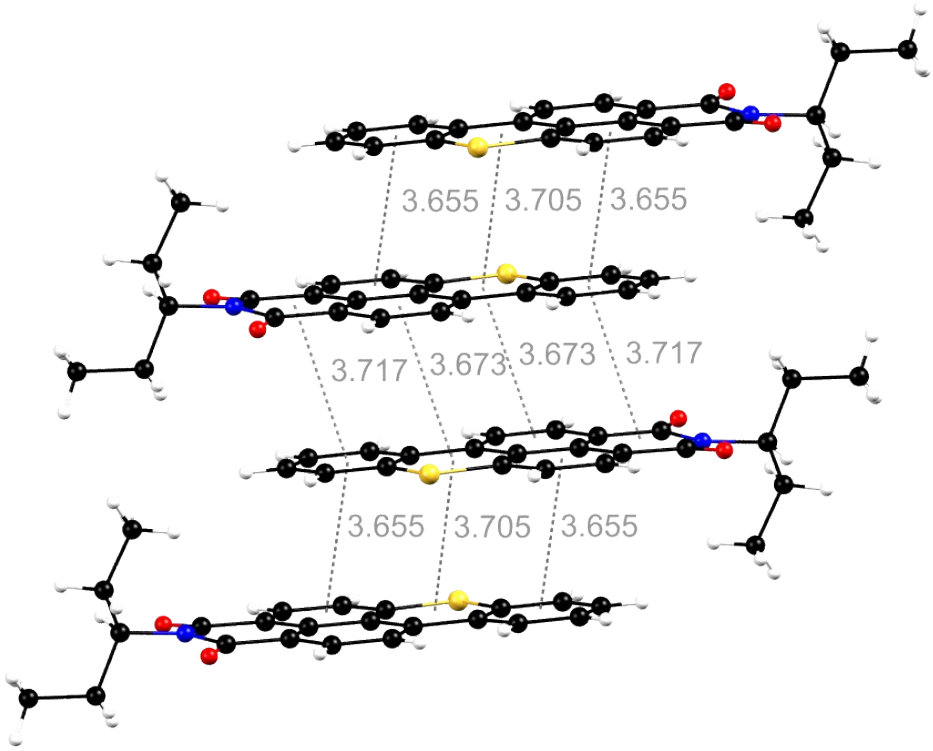

Figure S21. X-Ray structure of **D1** highlighting its π-π interaction distances in Å.

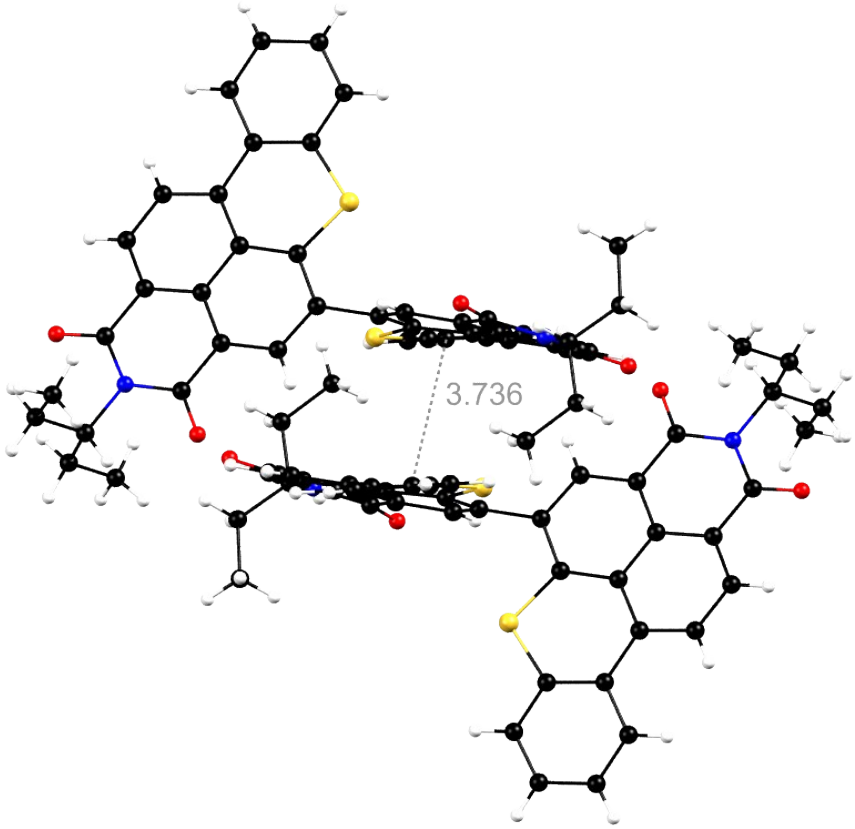

Figure S22. X-Ray structure of **D2** highlighting its π-π interaction distances in Å.

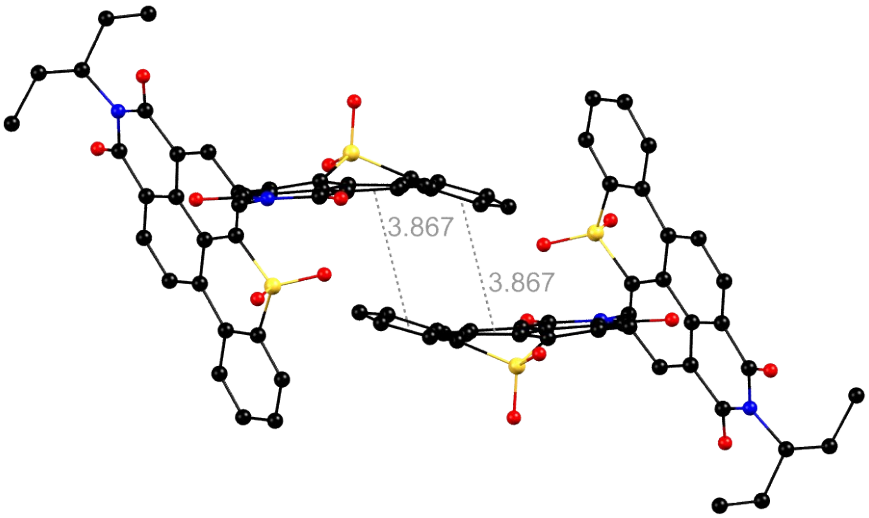

Figure S23. X-Ray structure of **D3** highlighting its hexameric toroidal structure where hydrogens and disorder have been omitted for clarity.

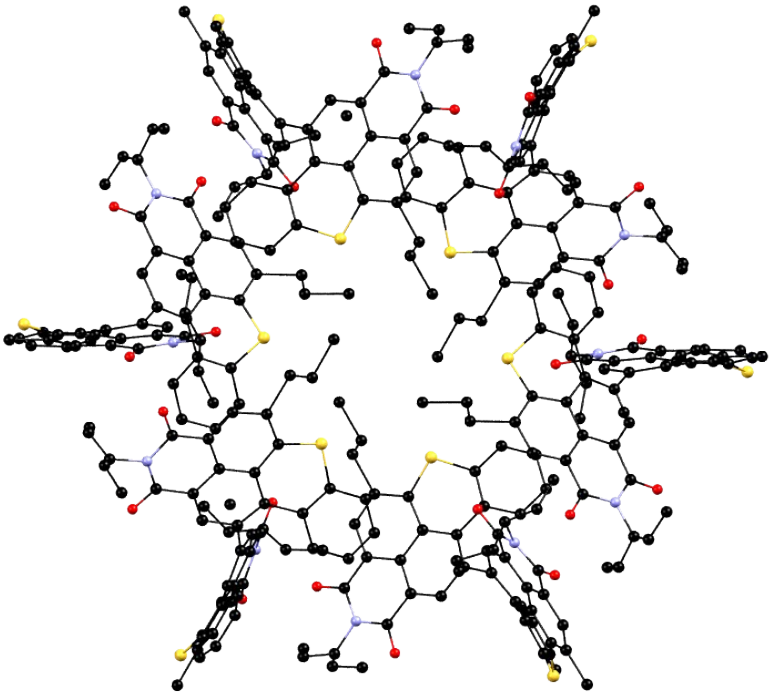

Figure S24. X-Ray structure of **D3** highlighting the π-π interactions between hexamers where hydrogens and disorder have been omitted for clarity.

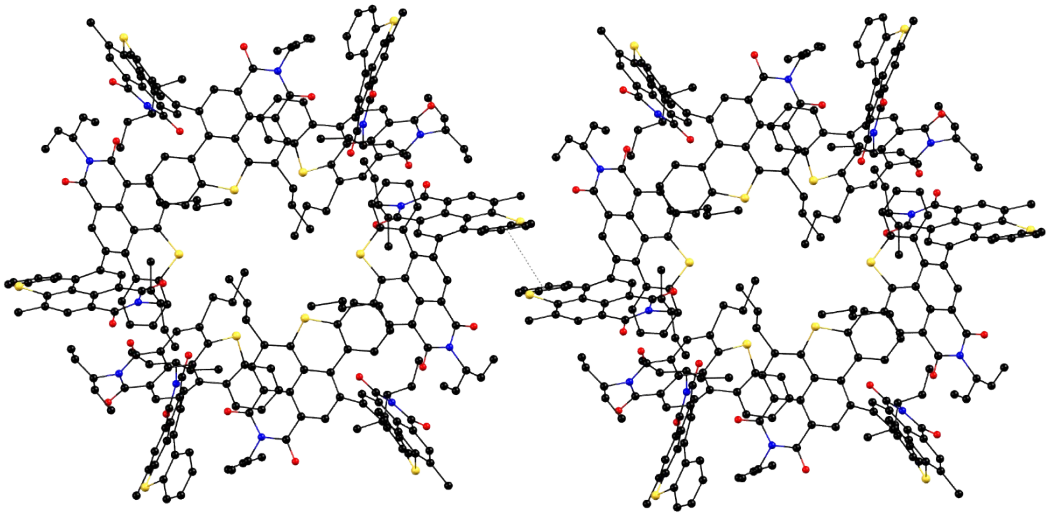

Figure S25. X-Ray structure of **D3** highlighting the π-π interaction distances in Å.

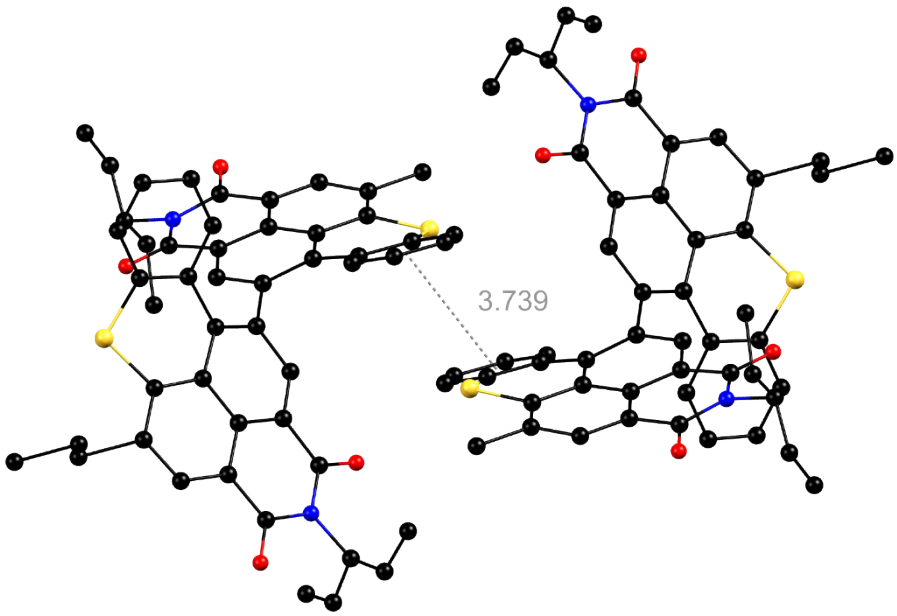

Crystallographic Data of BTXI-Alk, D1, D2 and D3

X-ray single-crystal diffraction data were collected at 150K on a Rigaku Oxford Diffraction SuperNova diffractometer equipped with an Atlas CCD detector and micro-focus Cu-K_α radiation (λ = 1.54184 Å). The structures were solved by dual-space algorithm, expanded and refined on F^2 by full matrix least-squares techniques using SHELX programs (G. M. Sheldrick, SHELXT 2018/2 and SHELXL 2018/3). All non-H atoms were refined anisotropically and multiscan empirical absorption was corrected using CrysAlisPro program (CrysAlisPro 1.171.40.45a, Rigaku Oxford Diffraction, 2019). The H atoms were placed at calculated positions and refined using a riding model.

The structure refinements of **D2** and **D3** showed disordered electron density which could not be reliably modeled and the program PLATON/SQUEEZE was used to remove the corresponding scattering contribution from the intensity data. This electron density can be attributed to solvent molecules (chloroform for **D2** and toluene for **D3**). The assumed solvent composition was used in the calculation of the empirical formula, formula weight, density, linear absorption coefficient, and F(000).

For **D1**, **D2** and **D3**, a statistical disorder was applied to lead to various occupation rates: for compound **D1,** two chloride atoms on one chloroform molecule with 0.603/0.397 occupancy factors; for compound **D2,** four ethylene parts with 0.545/0.455 and 0.577/0.423 occupancy factors and for compound **D3**, two ethylene parts with 0.627/0.373 occupancy factors and two isopropyl groups with 0.570/0.430 and 0.610/0.390 occupancy factors.

Crystallographic data for the four structures have been deposited with the Cambridge Crystallographic Data Centre, deposition numbers CCDC 2012963 for **BTXI-Alk**, 2012965 for **D1**, 2012966 for **D2**, 2012967 for **D3**. These data can be obtained free of charge from CCDC, 12 Union road, Cambridge CB2 1EZ, UK (e-mail: deposit@ccdc.cam.ac.uk or http://www.ccdc.cam.ac.uk).

Table S1 Data collection parameters for the resolved crystal structures of **BTXI-Alk, D1, D2 and D3**

Crystal	**BTXI-Alk**	**D1**	**D2**	**D3**
Formula	$C_{27}H_{27}NO_2S$	$C_{48}H_{38}Cl_6N_2O_4S_2$	$C_{47}H_{37}Cl_3N_2O_8S_2$	$C_{176}H_{172}N_6O_{12}S_6$
Molecular Weight	429.55	983.62	928.25	2755.55
Temperature (K)	150	150	150	150
Crystal system	Triclinic	Triclinic	Triclinic	Trigonal
Space group	*P*-1	*P*-1	*P*-1	*R*-3
a (Å)	7.1857(3)	9.3061(2)	10.6018(7)	45.615(2)
b (Å)	17.0238(5)	13.3044(3)	13.9495(8)	45.615(2)
c (Å)	19.6063(6)	18.0105(4)	15.1107(9)	12.3835(6)
α (°)	113.132(3)	83.284(2)	85.675(5)	90
β (°)	90.973(3)	87.291(2)	86.516(5)	90
γ (°)	96.562(3)	83.287(2)	74.883(5)	120
V (Å^3)	2186.1(1)	2198.16(9)	2149.3(2)	22315(2)
Z	4	2	2	6
Crystal color	yellow	yellow	yellow	orange
Crystal size (mm^3)	0.211 x 0.040 x 0.036	0.296 x 0.151 x 0.087	0.343 x 0.040 x 0.023	0.107 x 0.100 x 0.072
D_c (g cm^{-3})	1.305	1.486	1.434	1.230

μ (mm^{-1})	1.500	4.848	3.321	1.322
F(000)	912	1012	960	8772
Transmission (min/max)	0.8499/1.0000	0.8173/1.0000	0.8588/1.0000	0.8959/1.0000
θ (min/max) (°)	2.456/74.240	2.472/76.351	2.935/72.146	3.356/72.327
Data collected	16912	19226	15603	34107
Data unique	8462	8795	8018	9604
Data observed	6380	8213	5929	4663
R (int)	0.0304	0.0214	0.0504	0.0414
Nb of parameters	567	582	565	618
R_1 [I > 2σ(I)]	0.0467	0.0525	0.0766	0.1118
wR_2 [I > 2σ(I)]	0.1170	0.1434	0.1920	0.3372
R_1 [all data]	0.0594	0.0550	0.0986	0.1641
wR_2 [all data]	0.1264	0.1459	0.2057	0.3908
GOF on F^2	1.034	1.061	1.052	1.208
Largest peak in final: difference (e A^{-3})	0.733/-0.354	1.229/-0.689	0.620/-0.530	0.597/-0.393

Computational Chemistry

The gas-phase ground-state equilibrium geometry of representative molecules was obtained by performing DFT optimization at the range-separated hybrid (RSH) functional level of theory ωB97X-D[2] with the 6-31G(d,p) basis set for all the atomic species. The same levels of theory were used for all structural optimizations in *vacuum*. The influence of optimally tuning (OT) ω value (a key parameter in the class of RSH functionals) on the resulting optimized structures wes thereafter checked. To tune the ω value, a polarizable continuum model (PCM)[3] was used to take into account the electrostatic effects of the polarizable environment using a dielectric constant. The ω parameter was finely adjusted with PCM according to the "gap tuning" procedure[4,5] in order to accurately estimate (~ 50 meV of error) the energy of the frontier molecular orbitals. Ground-state population analysis was performed at the OT-RSH+PCM level of theory. Ultimately, as for the optical properties, OT-RSH+PCM TD-DFT calculations were carried out. All DFT and TD-DFT simulations were performed using the GAUSSIAN16 package suite.[6]

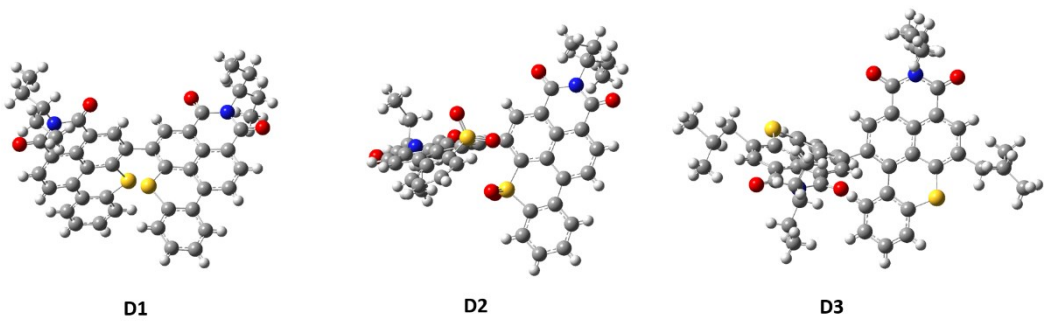

Figure S26. Optimized geometries of **D1**, **D2** and **D3**: DFT/OT-ωB97-XD/6-31G(d,p) /Dichloromethane (ε=8.9)

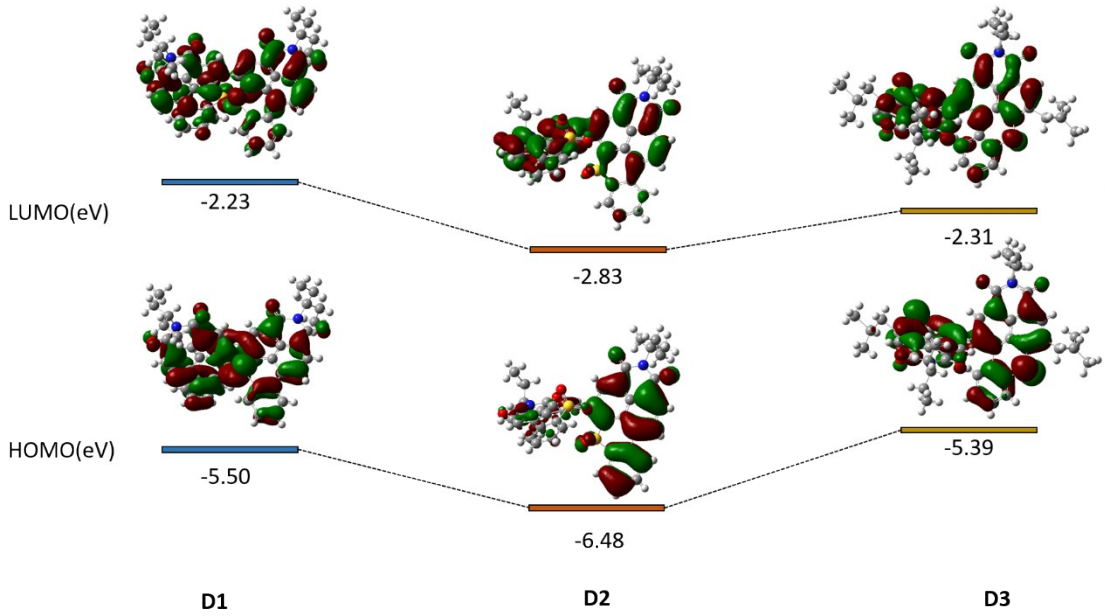

Figure S27. Simulated energy diagram and ground state population repartition

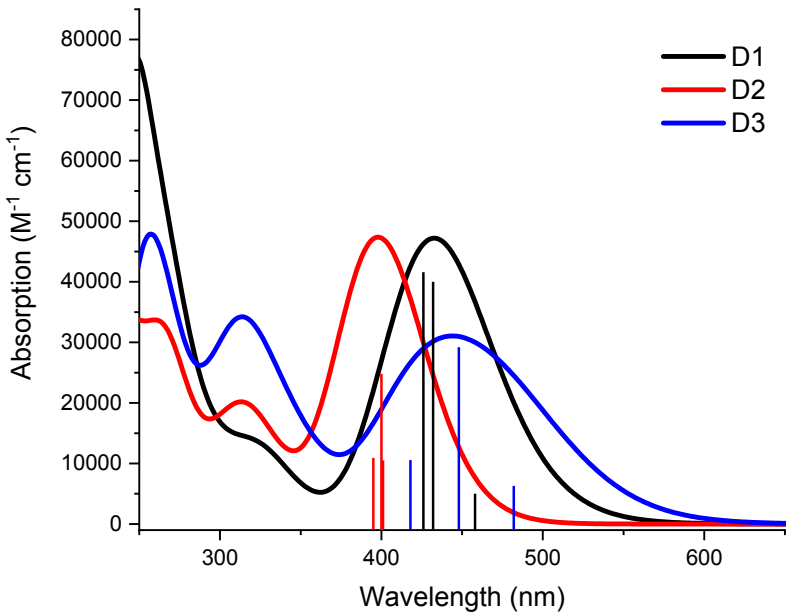

Figure S28. Simulated optical spectrum. TD-DFT/OT-ωB97-XD/6-31G(d,p) /Dichloromethane (ε=8.9)

Table S2. Simulated optical data. TD-DFT/OT-ωB97-XD/6-31G(d,p) /Dichloromethane (ε=8.9)

	wavelength (nm)	oscilator	transition major	transition minor
D1	458	0.13	HOMO->LUMO (74%)	H-1->L+1(26%)
	432	0.36	HOMO-1->LUMO (53%)	H->L+1 (47%)
	426	0.42	HOMO-1->LUMO+1 (68%)	H->L (19%), H-1->L (13%)
D2	401	0.19	HOMO->LUMO (66%)	H->L+1 (11%), H--1>L (23%)
	400	0.36	HOMO-1->LUMO (59%)	H->L+1 (21%), H->L (20%)
	395	0.19	HOMO->LUMO+1 (68%)	H-1->L (32%)
D3	482	0.26	HOMO->LUMO	-
	448	0.97	HOMO->LUMO+1 (55%)	H-1->L (45%)
	418	0.32	HOMO-1->LUMO+1	-

References

[1] aP. Josse, S. Li, S. Dayneko, D. Joly, A. Labrunie, S. Dabos-Seignon, M. Allain, B. Siegler, R. Demadrille, G. C. Welch, *Journal of Materials Chemistry C* **2018**, *6*, 761-766; bC. Dalinot, P. S. Marqués, J. M. Andrés Castán, P. Josse, M. Allain, L. A. Galán, C. Monnereau, O. Maury, P. Blanchard, C. Cabanetos, *European Journal of Organic Chemistry* **2020**; cL. A. Galán, J. M. A. Castán, C. Dalinot, P. S. Marqués, P. Blanchard, O. Maury, C. Cabanetos, T. Le Bahers, C. Monnereau, *Physical Chemistry Chemical Physics* **2020**.

[2] Chai, J.-D.; Head-Gordon, M. Long-Range Corrected Hybrid Density Functionals with Damped Atom–Atom Dispersion Corrections. *Phys. Chem. Chem. Phys.* **2008**, *10* (44), 6615–6620.

[3] Tomasi, J.; Mennucci, B.; Cammi, R. Quantum Mechanical Continuum Solvation Models. *Chem. Rev.* **2005**, *105* (8), 2999–3094.

[4] Stein, T.; Kronik, L.; Baer, R. Reliable Prediction of Charge Transfer Excitations in Molecular Complexesusing Time-Dependent Density Functional Theory. *J. Am. Chem. Soc.* **2009**, *131* (8), 2818–2820.

[5] Stein, T.; Kronik, L.; Baer, R. Prediction of Charge-Transfer Excitations in Coumarin-Based Dyes Using a Range-Separated Functional Tuned from First Principles. *J. Chem. Phys.* **2009**, *131* (24), 244119.

[6] M. J. Frisch, G. W. Trucks, H. B. Schlegel, G. E. Scuseria, M. A. Robb, J. R. Cheeseman, G. Scalmani, V. Barone, G. A. Petersson, H. Nakatsuji, X. Li, M. Caricato, A. V. Marenich, J. Bloino, B. G. Janesko, R. Gomperts, B. Mennucci, H. P. H. Gaussian 16. 2016.